Applications in Energy and Combustion Science 11 (2022) 100079

Contents lists available at ScienceDirect

Applications in Energy and Combustion Science

journal homepage: www.elsevier.com/locate/jaecs

Numerical prediction of research octane numbers via a quasi-dimensional two-zone cylinder model

Samuel Schlichting [a,*], Torsten Methling [a], Patrick Oßwald [a], Julia Zinsmeister [a], Uwe Riedel [b], Markus Köhler [a]

[a] Institute of Combustion Technology, German Aerospace Center (DLR), Pfaffenwaldring 38-40, 70569 Stuttgart, Germany
[b] Institute of Low-Carbon Industrial Processes, German Aerospace Center (DLR), Walther-Pauer-Straße 5, 03046 Cottbus, Germany

ARTICLE INFO

MSC:
00-01
99-00

Keywords:
Octane number
Two-zone cylinder model
Reactor network
Synthetic fuels

ABSTRACT

Sustainably produced synthetic fuels offer great potential for a fast reduction of the greenhouse gas emissions of the transport sector. For an immediate application within the existing infrastructure and vehicle fleet, synthetic fuels need to comply with existing standards such as the EN 228 for gasoline. Beyond these standards and with optimized fuel design, certain properties can be improved compared to conventional fuels. For this purpose, methods for evaluating the properties are needed.

This work discusses the development of a simplified numerical quasi-dimensional two-zone cylinder model, combined with chemical kinetic models, for the estimation of octane numbers. The model emulates fuel specific operating conditions of the standardized procedure for the determination of octane numbers in the cooperative fuel research engine with variable compression ratios. The two zones represent the burned and unburned in-cylinder volume and are modeled with homogeneous reactors. The octane numbers are determined by the identification of the critical compression ratio, for which premature ignition occurs in the unburned reactor.

A two-zone cylinder model is validated against experimental data for various primary reference fuels, blended with toluene, ethanol, isobutanol and ethyl *tert*-butyl ether. The successful application of different kinetic models is demonstrated and enables the application on a wide range of fuels. It is shown that the simulated research octane numbers are in good agreement with the experimental data.

1. Introduction

Synthetic fuels produced from sustainable sources offer a great potential for reducing the environmental impact in ground transport [1,2] and aviation sector [3–5] respectively the energy sector in general [6]. With drop-in fuels, the existing fuel infrastructure and vehicle fleet can be used, enabling quick integration into the established transportation system. Optimizing the composition of fuels can improve properties such as pollutant behavior and emissions, as well as engine performance and efficiency [1,7], which offers additional advantages over conventional fuels. This raises the question for tools assessing key features and optimizing possible fuel compositions.

One important index for the performance of fuels in spark-ignition (SI) engines is the octane number describing the fuel's tendency for self-ignition. These secondary ignitions in the residual fuel–air mixture, a condition known as engine knock, can lead to severe engine damage. The octane number is derived experimentally using the standardized procedure ASTM D2699 for the research octane number (RON) or ASTM D2700 for the motor octane number (MON). The measurement is performed in a cooperative fuel research (CFR) engine with an adjustable compression ratio and a defined set of operation conditions. The volumetric composition of the primary reference fuel (PRF), a mixture of isooctane and n-heptane, which exhibits the same ignition behavior respectively knock intensity determines the octane number.

Nevertheless, considerable amounts of fuel are required for these time-consuming, standardized tests. For an efficient fuel design process, it is therefore desirable to develop and provide alternative empirical and numerical methods for deriving the octane number including the ability to assess virtual fuel compositions.

Numerous approaches considering blending effects can already be found in the literature. Morgan et al. [8] use a 2nd order response surface method for mapping the composition of tri-component surrogates, blends of n-heptane, isooctane and toluene, to their octane numbers.

Lugo et al. [9] and Gosh et al. [10] describe models for correlating the research and motor octane numbers with fuel composition via a non-ideal model by dividing the individual species into groups according to their chemical properties. The detailed chemical composition of

* Correspondence to: German Aerospace Center, Pfaffenwaldring 38-40, 70569 Stuttgart, Germany.
E-mail address: samuel.schlichting@dlr.de (S. Schlichting).

https://doi.org/10.1016/j.jaecs.2022.100079
Received 30 May 2022; Received in revised form 26 July 2022; Accepted 3 August 2022
Available online 6 August 2022

the fuel in combination with the pure and blending octane numbers of the individual species are used by Nikolaou et al. [11] to calculate the octane number.

Tipler et al. [12] applied a Bayesian approach combined with a pseudo component method dividing the fuel in fractions of saturates, olefins, aromatics and oxygenates. For the training/calibration of the Bayesian approach, 45 test fuels are considered. Pal et al. [13] introduced a state of the art artificial neural network (ANN) model predicting the research as well as the motor octane number within a root mean square error of 1 ON unit. The application of machine learning models can be used to find further correlations between the octane number of the fuel and its compositions. In a deeper analysis of the individual species, the influences of individual structural groups and features can also be integrated and used to derive the octane number [14–16].

Both empirical models and machine learning models are capable of providing fast solutions to the posed problems. When new fuel-blends are considered, extending empirical models is challenging, since implementing new species requires great effort or is not even possible in a concept-based manner. Moreover, methods based on statistical data analysis and machine learning models require a large amount of training data. Also, the extrapolation of such models and their application to fuels with compositions and components outside the training-area provides challenges on its own.

Since octane numbers are related to the chemical kinetic process of auto-ignition, various numerical methods have been developed for the simulation of engines using chemical kinetic reaction mechanisms. Herein lies the key concept: the integration of fuel chemistry models that are ideally fuel flexible allow the coverage of a wide range of different fuels and components. For the numerical analysis of the ignition process, models with different levels of complexity can be applied to reproduce the boundary conditions in an internal combustion engine (ICE).

Simulations of ignition delay times in homogeneous zero-dimensional reactors enable the efficient applications of detailed chemical kinetic mechanisms, providing a good representation of the complex ignition path in the low temperature regime while maintaining short computing time. The resulting ignition delay time can be directly correlated to the octane number [17]. Westbrook et al. [18] implemented a method for predicting octane numbers using a predefined pressure profile instead of fixed constant boundary conditions for the simulation of ignition delay times. Fioroni et al. [19] applied this method to several four-component fuels and obtained good agreement with experimental data. Curran et al. [20] as well as Callahan et al. [21] use homogeneous reactor simulations with specific volume/time histories to calculate the critical compression ratios indicated by the onset of auto-ignition. The critical compression ratios are subsequently linked to the octane number. Zhang et al. [22] derive a volume profile based on a measured pressure profile from a CFR engine, which is used for simulations of ignition times in a homogeneous reactor. On the downside, all these methods based on simple zero-dimensional reactors necessitates predefined and fixed boundary conditions or dependents on given pre-defined volume or pressure profiles.

Computational fluid dynamics (CFD) simulations as described by Pal et al. [23,24], offer a more realistic reproduction of the boundary conditions in the cylinder with simulation of the velocity field including modeling of turbulence effects as well as a spatially resolved temperature distribution. This method requires high computational costs making it unfeasible to apply detailed chemical kinetic mechanisms replicating the low-temperature ignition path for fuel blends with multiple components.

Quasi-dimensional models dividing the cylinder into multiple zones offer a compromise between model accuracy and calculation costs. Compared to the simplified ignition delay time correlation approach, this method enables the simulation of different compression ratios including fuel depended compression effects of the residual fuel–air mixture caused by the propagation of the flame front and the burned gas. Nevertheless, certain model assumptions must be made regarding the propagation of the flame front and the heat losses.

Various approaches with two zones dividing the cylinder into a burned and unburned zone were suggested. Hajireza et al. [25] use a two-zone model for investigating the influence of gas homogeneity on the auto-ignition. They apply the Wiebe function for modeling the burning rate and incorporates a one-dimensional model in order to model a temperature profile towards the cylinder wall. Perini et al. [26] developed a model for evaluation of the performance and emissions of SI engines. For the burning rate the simplified assumption for a spherical propagating flame-front is made combined with the empirical correlation for the laminar burning velocity and an additional turbulence modeling. The model is calibrated for hydrogen methane blends. Foong [27] proposes a method for the simulation of the knock-point of toluene reference fuels blended with ethanol in a two-zone model using prescribed mass burning rates. The input are estimated using GT-power simulations [28] on bases of measured pressure profiles of the investigated fuel-blends. For the heat losses the Woschni [29] correlation is applied. The two-zone method is used by Mehl et al. [30] to determine the critical compression ratio marking the onset of self-ignition of hydrocarbon fuels.

In summary, numerical methods providing engine-related boundary conditions, must balance compromises between the required computational cost and model-based simplifications. Individual calibrations for various engine operating parameters are necessary, but the application to a vast variety of fuels and compositions is limited only by the used chemical kinetic mechanism. The mechanisms are independent of the engine model and can be exchanged or extended and finally validated using basic chemical experimental data, such as ignition delay times measured with rapid compression machines.

With the motivation of simplifying the fuel design process for synthetic fuels, this work focuses on the development of a model for the prediction of octane numbers for a wide range of future fuels with either complex compositions or novel molecules.

Predicting octane numbers for a wide range of fuels makes fuel-specific model calibration infeasible. Therefore, the introduced model is designed and validated without the need of individual calibration and is not dependent on given fuel specific experimentally derived input-data like pressure profiles. In addition, for great fuel flexibility, the model is designed to allow the chemical kinetic mechanisms to be interchangeable.

The flexibility in the mechanism selection can be utilized, to focus on oxygenated fuel components with the capability of boosting the octane number, making their application as additives attractive. Additionally, many Fischer–Tropsch (FT) fuels tend to contain a high proportion of unbranched alkanes [31,32], thus FT fuels usually exhibit octane numbers that are too low for the application in SI engines. With modern fuel design strategies, this can be improved by extensive isomerization treatment and the addition of octane boosters.

As a basis for the implementation of the model, a simplified two-zone approach is chosen dividing the cylinder in a burned and unburned zone offering the best compromise of computational cost and accuracy. Compared to single-zone models, the approach of treating the burned and unburned zones separately enables the better representation of the conditions in SI engine such as compression effects caused by the burned gas. Furthermore, a fuel specific burn rate is implemented in the model by combining a calibrated flame surface including turbulence effects and individual laminar flame velocities and densities. The flame surface area is derived via a calibration process while the fuel specific laminar flame speeds are preliminary modeled and tabulated. The density as a variable of state is also available. Therefore the model is able to provide engine related boundary conditions for specific fuels without the need of recalibration using experimental data.

The general structure of the model is based on a network of homogeneous reactors. Consequently, the model cannot provide the direct

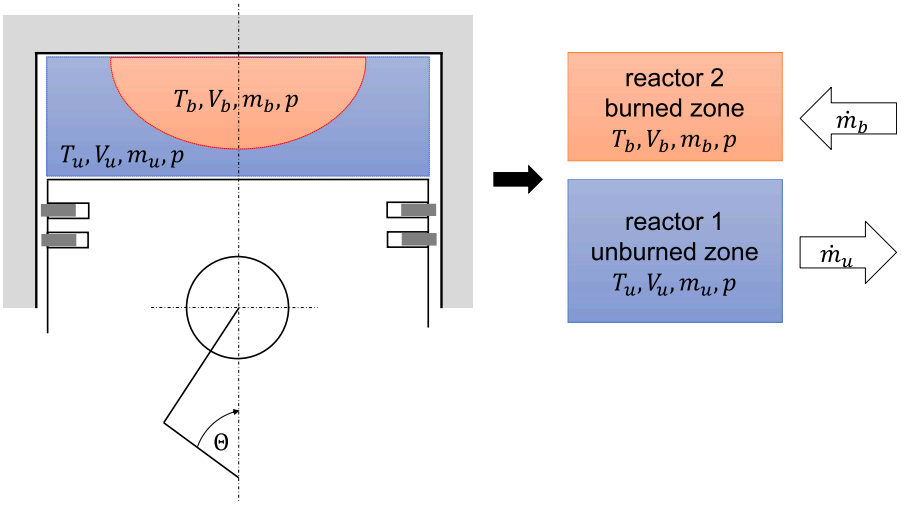

Fig. 1. Visualization of the 2-zone-cylinder-model's structure. The zones with the fresh unburned fuel–air mixture and the burned gas are represented by two homogeneous reactors exhibiting individual gas states. The pressure conditions are assumed to be equal in both zones. The propagation of the flame front is modeled by the mass flow leaving the unburned zone and being supplied to the burned zone.

determination of the octane number via the knock intensity as in the standardized experimental setup. Instead, the model is designed to determine critical compression ratios by detecting secondary self-ignition in the unburned zone through the application of detailed chemical kinetic mechanisms covering the low-temperature range. Based on these simulated compression ratios, correlations are established for the numeric prediction of research octane numbers (RON).

The development of the quasi-dimensional model is discussed in detail in the following section, including the definitions concerning the propagation of the flame front as well as the determination of the wall heat losses.

2. Two-zone cylinder model

This work focuses on the development of a two-zone cylinder model for the prediction of octane numbers with the Cantera library [33] using the quasi-dimensional model approach. With the intention of replicating the standardized experimental procedure, a correlation based on the critical compression ratio (CCR) is established using chemical kinetic self-ignition simulations. The model is designed to provide engine-relevant boundary conditions with variable compression ratios. The influence of the fuel properties is addressed as well.

Following the quasi-dimensional approach, the combustion chamber is divided into two zones, one for the burned gas (index b) and one for the unburned (index u) fuel–air mixture. Fig. 1 visualizes the model structure. Both zones are simulated by two homogeneous reactors with variable pressure and volume conditions which are linked together by the flame front. The propagation of the flame is represented by the unburned gas taken out of the first reactor while the same mass of burned gas is fed into the second reactor. The closed system, with the exception of the wall heat losses, necessitates the accounting of energy conservation in addition to mass conservation. The compression work introduced to the system respectively to the unburned fuel–air mixture by the engine piston also must be attributed to the gas fed into the burned reactor. Any blow-by gases e.g., between the piston and cylinder wall entering the crankcase are neglected.

A constant pressure field is assumed throughout the cylinder. An implemented "moving wall" controls the volume fractions of the two zones to achieve a pressure equilibrium regarding the conditions of the gas phases. The lack of spatial resolution of the zones and the resulting constant temperature field prohibit the formation of a temperature gradient from the cylinder wall to its center caused by wall heat losses. To overcome this restriction, the adiabatic core hypothesis is applied assuming that the layer close to the wall cools down due to the heat flow. The resulting pressure drop leads to an expansion of the gas in the center and thus to a temperature drop which can be described by an isentropic expansion. This modeling approach for the cylinder core temperature is also applied for the modeling of rapid compression machines [34].

The governing equations of the two-zone model are based on a set of conservation and state equations. The energy conservation equations for the two reactors, with the subscript u representing the unburned reactor and the subscript b representing the burned reactor, can be formulated as follows [35]:

$$m_{\mathrm{u}} c_{v,\mathrm{u}} \frac{dT_{\mathrm{u}}}{dt} = -p\frac{dV_{\mathrm{u}}}{dt} - \frac{pV_{\mathrm{u}}}{m_{\mathrm{u}}}\frac{dm_{\mathrm{u}}}{dt} - \sum_s \dot{m}_{s,\mathrm{gen,u}} u_{s,\mathrm{u}}, \tag{1}$$

$$m_{\mathrm{b}} c_{v,\mathrm{b}} \frac{dT_{\mathrm{b}}}{dt} = -p\frac{dV_{\mathrm{b}}}{dt} + \frac{dm_{\mathrm{b}}}{dt}(h_{\mathrm{in}} - \sum_s u_s Y_{s,\mathrm{in}}) - \sum_s \dot{m}_{s,\mathrm{gen,b}} u_{s,\mathrm{b}}, \tag{2}$$

where the reactor specific mass m, volume V and temperature T as well as their time depended derivatives are included. The specific heat capacity c_v, the species specific internal energy u_s with $Y_{s,\mathrm{in}}$ in Eq. (2) providing the mass fraction of each species s entering the burned reactor. $\dot{m}_{s,\mathrm{gen}}$ is the change of mass of each species s due to the reactions and is derived from the chemical kinetic mechanism.

Using the ideal gas equation with the molar mass M for the individual reactors specified, the following equations can be derived for the pressure change in the reactor network:

$$\frac{dp}{dt} = \frac{RT_{\mathrm{u}}}{V_{\mathrm{u}} M_{\mathrm{u}}} \cdot \frac{dm_{\mathrm{u}}}{dt} - \frac{RT_{\mathrm{u}}}{V_{\mathrm{u}} M_{\mathrm{u}}^2} \cdot \frac{dM_{\mathrm{u}}}{dt} + \frac{m_{\mathrm{u}} R}{M_{\mathrm{u}} V_{\mathrm{u}}} \cdot \frac{dT_{\mathrm{u}}}{dt} - \frac{m_{\mathrm{u}} RT_{\mathrm{u}}}{M_{\mathrm{u}} V_{\mathrm{u}}^2} \cdot \frac{dV_{\mathrm{u}}}{dt}, \tag{3}$$

$$\frac{dp}{dt} = \frac{RT_{\mathrm{b}}}{V_{\mathrm{b}} M_{\mathrm{u}}} \cdot \frac{dm_{\mathrm{b}}}{dt} - \frac{RT_{\mathrm{b}}}{V_{\mathrm{b}} M_{\mathrm{u}}^2} \cdot \frac{dM_{\mathrm{b}}}{dt} + \frac{m_{\mathrm{b}} R}{M_{\mathrm{b}} V_{\mathrm{b}}} \cdot \frac{dT_{\mathrm{b}}}{dt} - \frac{m_{\mathrm{b}} RT_{\mathrm{b}}}{M_{\mathrm{b}} V_{\mathrm{b}}^2} \cdot \frac{dV_{\mathrm{b}}}{dt}, \tag{4}$$

enabling the incorporation of a given pressure profile.

The volume change of the reactor network is mainly dictated by the motion of the engine piston dV_{piston}/dt acting on the unburned dV_{u}/dt and burned dV_{b}/dt reactor. Combined with the isentropic expansion dV_{hl}/dt for the modeling of the wall heat losses, the following equation is obtained:

$$\frac{dV_{\mathrm{network}}}{dt} = \frac{dV_{\mathrm{u}}}{dt} + \frac{dV_{\mathrm{b}}}{dt} = \frac{dV_{\mathrm{piston}}}{dt} + \frac{dV_{\mathrm{hl}}}{dt}. \tag{5}$$

The formulated mass flow reflects the burning rate. For the reactor network the total mass flow equals zero in order to fulfill the mass conservation:

$$\frac{dm}{dt}_{\mathrm{network}} = \frac{dm_{\mathrm{u}}}{dt} + \frac{dm_{\mathrm{b}}}{dt} = 0, \tag{6}$$

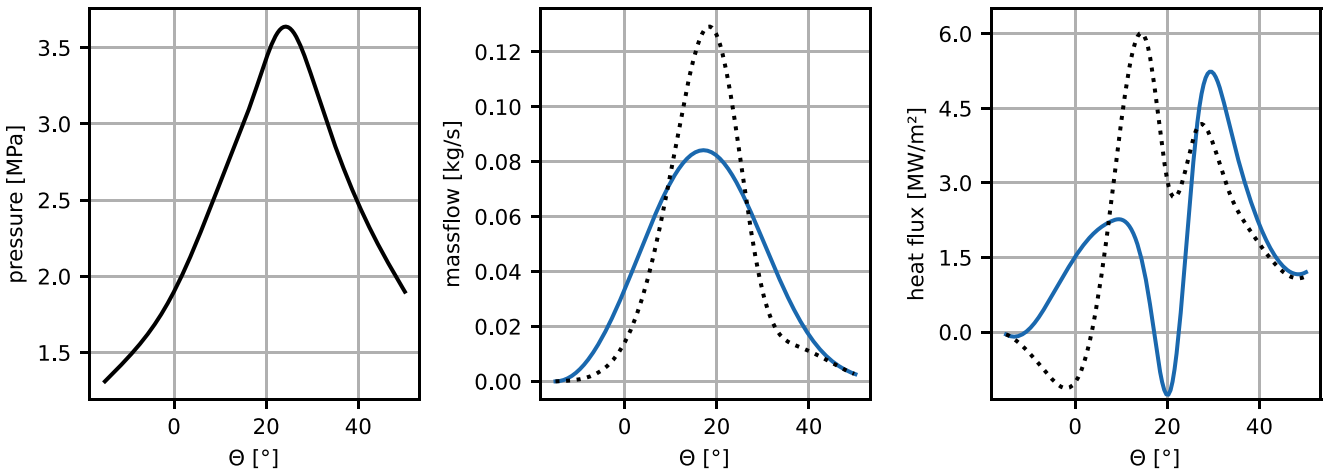

Fig. 2. Left: Pressure profile for the calibration of the model. Middle: Mass conservation calculated using the single Wiebe function (blue line) respectively the double Wiebe function (black dotted line). Right: The calculated heat flux for both, single and double Wiebe function is visualized.

leading to the condition $-\dot{m}_u = \dot{m}_b = \dot{m}$.

The 6 governing Eqs. (1)–(6) of the two-zone model involve 8 unknown quantities: dT_u/dt, dT_b/dt, dp/dt, dm_u/dt, dm_b/dt, dV_u/dt, dV_b/dt, dV_{hl}/dt. In order to solve this system of equations two quantities need to be modeled. Hence, dm/dt and dV_{hl}/dt are modeled with simplified assumptions and calibrated with experimental results of a pressure profile from a CFR engine also used by Zhang et al. [22] for their single zone model. This pressure profile was derived while burning PRF100 under stoichiometric conditions, a compression ratio of 9.21 and a ignition timing of 15 crank angle degree (CAD) before top dead center (BTDC). The initial pressure at the time when the inlet valve is closed is 1.09 bar. These boundary conditions are also chosen for the setup of the new implemented model. Since the experiments in the CFR engine are performed at the lambda of the highest knock intensity which is usually on the rich side of stoichiometry, the performance of the model was tested at ϕ 1.1. The results given in the supplementary material show no significant difference between the stoichiometric mixtures chosen in this work and mixtures with ϕ 1.1. The ignition timing used in the experimental pressure profile at 15 CAD BTCD deviates from the standardized ignition timing at 13 CAD BTCD. A comparison between the two ignition timings reveals no significant difference in the predictive ability of the model. The intake temperature is specified to 325 K according to the standardized procedure for the research octane number. Since the simulation starts at 146 CAD BTCD at the time the intake valve closes, it is reasonable to assume that the fuel–air mixture is already heated. The initial temperature of 350 K has been found to yield good results for the performed simulations. Further physical effects regarding cooling effects due to fuel specific enthalpies of vaporization were not considered. The details of the calibration process are given in the following sections.

2.1. Modeling wall heat losses and mass-transfer through the flame front

As demonstrated before, for the successful implementation of the two-zone approach, assumptions and definitions regarding the mass flow and the quantification of the heat losses are necessary.

The Wiebe function provides a simple method to quantify the mass transport from the unburned to the burned zone [25,36]:

$$\frac{dm}{d\Theta} = \frac{m_{\text{total}}}{\Delta\Theta} \cdot a(n+1) \left(\frac{\Theta - \Theta_{\text{ignition}}}{\Delta\Theta}\right) \cdot \exp\left(-a\left(\frac{\Theta - \Theta_{\text{ignition}}}{\Delta\Theta}\right)^{n+1}\right). \quad (7)$$

This approach incorporates the onset $\Theta_{ignition}$ and duration $\Delta\Theta$ of combustion as well as a shape factor n to fit the model to experimental data. The factor a is given as follows:

$$a = -ln(1 - \eta_{u,\text{ges}}), \quad (8)$$

with $\eta_{u,\text{ges}}$ describing the degree of mass conversation.

The application of the Wiebe functions for the missing burning rate $\dot{m}$ in combination with Eq. (4) and the given experimental pressure profile [22], plotted on the left in Fig. 2 allows the calculation of the wall heat losses. The resulting heat flux, displayed in the right diagram of Fig. 2, exhibits an physically unlikely behavior for the heat losses. For negative values, it indicates that energy is flowing into the system, leading to the conclusion that the adaptation of the Wiebe function with the applied calibration respectively chosen shape factor n is an oversimplification.

A more capable double-Wiebe function [37] for the burned fraction x_b can be used to approximate the slower burn duration near the wall

$$\frac{dx_b}{d\Theta} = (1 - a_{\text{wall}}) \cdot \left(\frac{a(n+1)}{\Delta\Theta} \cdot \left(\frac{\Theta - \Theta_{\text{ign}}}{\Delta\Theta}\right) \cdot \exp\left(-a\left(\frac{\Theta - \Theta_{\text{ign}}}{\Delta\Theta}\right)^{n+1}\right)\right) + a_{wall} \cdot \left(\frac{a(n+1)}{k_{\text{wall}}\Delta\Theta} \cdot \left(\frac{\Theta - \Theta_{\text{igh}}}{k_{\text{wall}}\Delta\Theta}\right) \cdot \exp\left(-a\left(\frac{\Theta - \Theta_{\text{ign}}}{k_{\text{wall}}\Delta\Theta}\right)^{n+1}\right)\right). \quad (9)$$

Within this approach, the fraction a_{wall} of the fuel–air mixture with a slower burning duration is introduced, as well as the ratio k_{wall} of the slower burning duration compared to the standard burning duration. Fig. 2 shows that the implementation of the double-Wiebe function allows a closer representation of the real engine burning rate. The resulting wall heat losses are still physically unlikely with the appearance of negative heat losses and two local maxima.

Alternatively, the mass flow from the unburned into the burned gas can be described by:

$$\frac{dm_b}{dt} = \rho_u \cdot A_f \cdot u_l, \quad (10)$$

involving the density ρ_u of the unburned gas phase, the flame surface area A_f and the laminar burning velocity u_l. In the model ρ_u is defined by the state variables. To estimate the fuel dependent u_l, fuel specific burning velocities are simulated and tabulated for the relevant pressure and temperature range of the engine. A_f is defined by the flame front propagation and the intensity of turbulence. Since these information are not available within homogeneous reactor models, the definition of A_f needs to be simplified in the two-zone model. With the execution of a calibration test case using an experimental pressure profile as well as the premise of known wall heat losses, the burning rate dm_b is determined. Combined with the laminar burning velocity of the test fuel A_f is estimated as a function of the relative volume $V_{b,\text{rel}}$ of the burned gas:

$$V_{b,\text{rel}} = V_b / V_{\text{network}}. \quad (11)$$

With this simplified approach, it is assumed that all information about the in-cylinder turbulence field are included in A_f. Due to the simplification requirements, the function of A_f is held constant as fuel dependent effects like the intensity of turbulence need to be neglected. The subsequent recombination of the flame surface A_f with the specific density and laminar burning velocity of the candidate fuel results in a fuel-specific burn rate. The calibration test case and method are discussed in the following section.

The wall heat losses, modeled by the isentropic expansion dV_{hl}/dt in Eq. (5), are also dependent on the flow conditions in the cylinder and need to be simplified for the same reasons as for the mass flow modeling. In general, the heat flux $\dot{Q}$ from a fluid with the temperature T_2 to a wall with the temperature T_1 is given by:

$$\dot{Q} = hA(T_2 - T_1), \tag{12}$$

for which h is the heat transfer coefficient and A is the contact area. The heat flux is proportional to the fluid temperature. The variables h and A are dependent on the turbulent flow field and position of the flame front. The position of the flame front defines the contact areas of the fluids of the two modeled zones with the temperatures T_{b} and T_{u}, as illustrated in Fig. 1. Since information on the turbulent flow field and the flame front position are not available in the homogeneous reactor model, a simplified heat loss model needs to be assumed:

$$\frac{dV_{\mathrm{hl}}}{dt} = \frac{f_{\mathrm{sig,d}}(V_{\mathrm{b,rel}}) \cdot \left(f_{\mathrm{sig,u}}(V_{\mathrm{b,rel}}) \cdot (T_{\mathrm{u}} - \overline{T}_{\mathrm{w}}) + f_{\mathrm{sig,b}}(V_{\mathrm{b,rel}}) \cdot (T_{\mathrm{b}} - \overline{T}_{\mathrm{w}}) \right)}{p}, \tag{13}$$

with the averaged wall temperature $\overline{T}_{\mathrm{w}}$ and the sigmoid function:

$$f_{\mathrm{sig,i}}(x) = \frac{a}{1 + \exp(-b \cdot (x - c))}. \tag{14}$$

The constants a_{u} and a_{b} represent the factors $h_{\mathrm{u}}A$ and $h_{\mathrm{b}}A$. The constants b and c define the position and maximum of the slope of the sigmoid functions. The transition of the contact area caused by the propagating flame front, is designed by the constraints:

$$b_{\mathrm{u}} = -b_{\mathrm{b}}, \tag{15}$$

$$c_{\mathrm{u}} = c_{\mathrm{b}}. \tag{16}$$

Measurements of the heat flux indicate a decrease in the heat losses towards the end of the engine's power cycle [38]. To account for this effect the damping sigmoid function $f_{\mathrm{sig,d}}$ is added in Eq. (13).

The constants of the sigmoid functions as well as $\overline{T}_{\mathrm{w}}$ are also estimated with the calibration test case, presented in the next section. Due to discussed simplification requirements, these parameters are held constant as fuel dependent effects like the intensity of turbulence need to be neglected.

2.2. Calibration of the two-zone cylinder model

In order to solve the governing equations of the two-zone model two from the three quantities dp/dt, dm/dt and dV/dt must be given as input to the model. As mentioned before, for the applied determination the CCR dm/dt and dV/dt_{hl} are scaled from a calibration reference case. In this calibration case dp/dt is taken from an experimental pressure profile [22] measured and averaged over 500 cycles in a CFR engine running under RON conditions with PRF100. Subsequently, dm/dt and dV/dt are determined with a optimization problem. In this optimization problem, the calibration factors from Eq. (13) are the input parameters and the profiles $m(t)$, dm/dt and d^2m/dt^2 are the output parameters for the objective function.

To solve the optimization problem, a genetic algorithm (GA) [39] is applied. The individuals of the GA are formed by different sets of the input parameters from Eq. (13). The initial population is formed by 48 individuals and $m(t)$, dm/dt and d^2m/dt^2 are evaluated by a fitness function. Each following generation of 32 individuals is derived by mutations of the five individuals with the best fitness. The goal of the mutations is to achieve better individuals by subtle changes in the parameters of already good parameter sets. Therefore, a normal distribution is applied, using the input parameters of the parents as median and 10% of the valid parameter range as variance.

For the evaluation of the overall fitness following function is introduced:

$$f = \sum_{\mathrm{i}} a_{\mathrm{i}} \cdot f_{\mathrm{i}}, \tag{17}$$

which sums up the fitness over all defined criterion i. Via the factor a_{i}, the possibility is given to prioritize each criteria independently. The target of the genetic algorithm is to minimize the objective function (17).

In order to define the fitness, five criteria are introduced evaluating the mass $m(t)$, the burn rate dm/dt as well as the second derivative d^2m/dt^2. The target for the mass as well as for its first and second derivative is to tend towards zero at the end of the engine cycle:

$$m_{\mathrm{u}}(t) = 0|_{t=t_{\mathrm{end}}}, \tag{18}$$

$$\frac{dm_{\mathrm{u}}}{dt} = 0|_{t=t_{\mathrm{end}}}, \tag{19}$$

$$\frac{d^2m_{\mathrm{u}}}{dt^2} = 0|_{t=t_{\mathrm{end}}}. \tag{20}$$

For these first three criteria, the deviations of the actual values compared to their targets are evaluated as the objective function to be minimized. For the evaluation process the deviation is adjusted by the multiplication with the factor a_{i} from Eq. (17).

The mass flow is a unidirectional quantity, since no burned gas can return to the unburned zone. Hence, the mass flow must be greater than zero during the engine cycle:

$$\frac{dm}{dt} > 0 \quad \text{for} \quad t_{\mathrm{start}} < t < t_{\mathrm{end}}. \tag{21}$$

The fifth objective relates to the mass flow rate and the number of maxima it exhibits. The idea is that the mass flow respectively burn rate accelerates until it reaches the maximum and then decelerates again as the flame extinguishes in the boundary layer near the wall. To avoid multiple maxima, the derivative of the firing rate $\ddot{m}$ after the first maximum t_{maxima} must remain below zero:

$$\frac{d^2m}{dt^2} < 0 \quad \text{for} \quad t_{\mathrm{maxima}} < t < t_{\mathrm{end}}. \tag{22}$$

To implement the constraints from the fourth and fifth criterion in Eq. (17), a sigmoid function is used, which is equivalent to Eq. (14). The parameters of the sigmoid function are designed, so that a penalty value is only added to the fitness function in Eq. (17), when the constraint is violated.

Fig. 3 visualizes on the left the simulated pressure profile of the performed calibration process. In the middle plot the determined burn rate is displayed and compared with the burn rate calculated using the double Wiebe approach indicated by the black dashed line. Toward the end of the cycle the derived burn rate exhibits a slower burn duration due to wall effects, which is also described by the double Wiebe function. The gradient of the derived combustion rate in the direction of the peak value, by contrast, is significantly steeper, which indicates a significantly faster propagation of the flame front. The corresponding heat flux is plotted on the right side, again in comparison to the black dashed line indicating the heat flux of the simulation with the combustion rate derived from the double Wiebe function, as discussed earlier. The new heat flux is now plausible and resembles in its progression and magnitude the wall heat flux of a SI motor measured by Han et al. [38]. It should be noted that different engine parameters and fuels were used in the experimental measurements. Furthermore, it is shown by Han et al. [38], that the propagation of the flame front in a real engine will cause a varying heat flux depending on time and location in the cylinder. Due to the simplicity of the quasi-dimensional

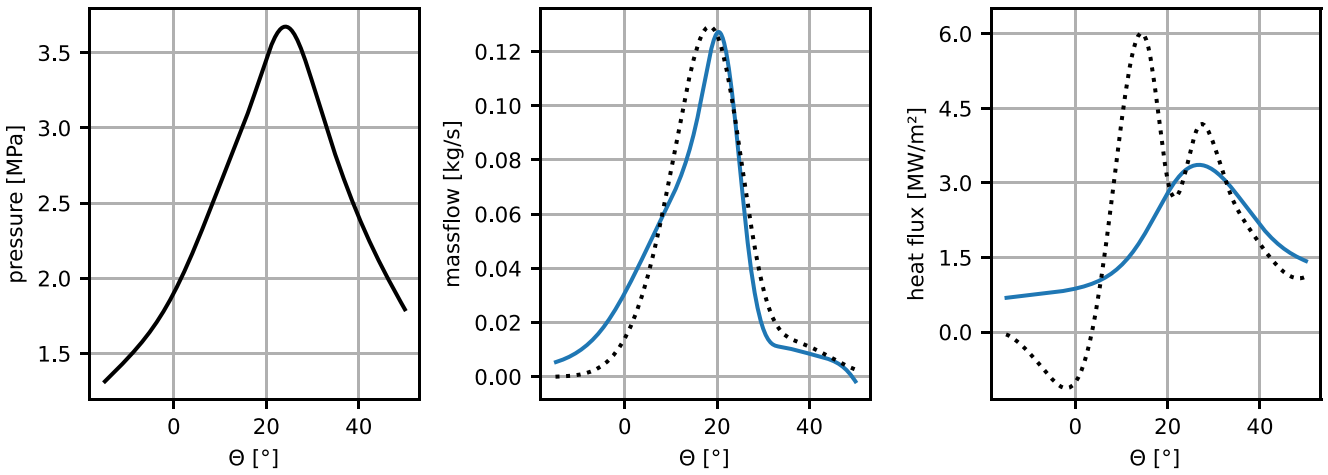

Fig. 3. Left: Pressure profile for the calibration of the model. Middle: Mass conservation derived via the genetic algorithm (blue line) as well as the burn rate calculated using the double Wiebe function (black dotted line). Right Heat flux derived using the genetic algorithm (blue line) and the resulting heat flux using the double Wiebe function (black dotted line).

approach with its lack of spatial resolution the profile of the derived wall heat flux and the peak value at around 20 degree after top dead center has to be considered as an over the entire cylinder averaged quantity.

2.3. Fuel blends and suitable chemical kinetic mechanisms

To validate the two-zone cylinder model, experimentally obtained octane numbers from various fuel blends were collected from literature, and are listed in Table 1. The list contains primary reference fuels (PRF) and toluene primary reference fuels (TPRF) mixtures, as well as blends of these reference fuels with alcohols and ethers, to cover a wide range of typical gasoline compositions. Oxygenates are of special interest for boosting octane number in renewable synthetic fuels, which enables potentially the improvement of thermal efficiency of spark ignition engines. The exact composition of the blends in Table 1 is given in the Supplementary Material.

Secondary self-ignitions in ICE leading to engine knock appear at temperatures below 1000 K. Therefore, the selected chemical-kinetic models need to be validated for low temperature ignition regimes [30]. The selected models for the simulations come from the Lawrence Livermore National Laboratory (LLNL) using two versions of the gasoline surrogate mechanism LLNL 2012 (ver. 1.0 2012-03-30) and LLNL 2020 (R20200313) [40,41]) as well as the TPRF model by POLIMI with the addition of submodels for alcohols and ethers (Version 2003, March 2020) [42] labeled as POLIMI 2020 in this work. All mechanisms are validated for the combustion of PRF, TPRF as well as ethanol (EtOH). In addition, the LLNL 2020 model is used to evaluate TPRF mixtures with isobutanol (iBuOH). The POLIMI 2020 model is applied to evaluate the PRF mixtures with ethyl *tert*-butyl ether (ETBE).

For the demonstration of real fuel predictability, fuels from Zinsmeister et al. [2] were selected and are listed in Table 2. The fuels comply with the European specification EN 228 and therefore offer a drop-in option. The only exception is the blend designated as E30 with 30 vol.% ethanol, which exceeds the limitations and can therefore not be easily applied as an drop-in fuel in the current vehicle fleet. Also included in the list is a conventional fossil reference fuel RefEU5.

The iBuOHmax fuel was designed to maximize the content of sustainably produced isobutanol with 14.5 vol.% while maintaining the limitations set by EN 228. The fuel blend, labeled as ReMax, is designed to contain the maximum amount of renewable components including ETBE and a FT surrogate. The fuel designated ETBEmax contains 22 vol.% ETBE. The FT(20)ETBE fuel has an additional FT content of 20 vol.%.

Table 1
Surrogates used for critical compression ratio simulations to either establish or validate a CCR-RON correlation. The octane numbers for these surrogates are found in the literature or, in the case of PRF, can be defined by the volumetric composition. The range of RON covered in this study is from 0 to nearly 110, while for the validation the range above 90 RON is of particular interest with respect to the application in SI engines.

ID	Fuel	Admixture	Source	Application
1	PRF;	–	–	Correlation
	PRF91-EtOH	80 vol.% EtOH	[27]	Correlation
2	TPRF	–	[8]	Validation
3	PRF - EtOH	10–80 vol.% EtOH	[27]	Validation
4	TPRF91-15 – EtOH	10–80 vol.% EtOH	[27]	Validation
5	TPRF91-30 – EtOH	10–80 vol.% EtOH	[27]	Validation
6	TPRF91-45 – EtOH	10–80 vol.% EtOH	[27]	Validation
7	PRF80 – iBuOH	0–30 vol.% iBuOH	[43]	Validation
8	TPRF80 – iBuOH	0–40 vol.% iBuOH	[43]	Validation
9	PRF – ETBE	5–15 vol.% ETBE	[44]	Validation

The composition as well as physical properties and combustion chemistry of these fuels are discussed by Zinsmeister et al. [2].

The composition of the fuels is given within the chemical classes: n-paraffins, iso-paraffins, naphthenes, aromatics, olefins as well as alcohols and ethers. In order to simulate the critical compression ratio and subsequently the octane number, the surrogate strategy by Kathrotia et al. [45] is applied. With this strategy approach, the individual chemical classes are matched due to the selection of class representative molecules in a given chemical kinetic reaction mechanism. By selecting multiple representative molecules from the mechanism, the hydrogen carbon ratio within a class can be matched. The exact compositions of the surrogates are shown in the Supplementary Material.

2.4. Correlation CCR-RON

In order to predict octane numbers, the octane number needs to be correlated with the simulated CCR. Subsequently, the derived correlation can be used to predict the octane numbers of the fuels listed in Table 1. The critical compression ratio marks the beginning of secondary spontaneous combustion in the unburned zone and is detected by the associated temperature rise.

The fuels used for establishing the correlation are PRF blends with varying isooctane proportions covering the range from zero to 100 RON. In order to extend the correlation's scope for fuels with an octane number greater than 100, a PRF91 blended with 80 vol.% ethanol resulting in an octane number of 108.4 [27] is added to the process.

Table 2
Fuels according to Zinsmeister et al. [2]. All listed fuels comply with the limits of EN 228, with the exception of E30 with an ethanol content of 30 vol.%.

Fuel	Specification, blending components
RefEU5	EN 228 compliant fossil reference fuel
E30	Non-standard compliant blend, ethanol (30 vol.%)
iBuOHmax	EN 228 compliant blend, isobutanol (14.5 vol.%)
ReMax	EN 228 compliant blend, ETBE (22 vol.%), FT-Surrogate (18 vol.%), isooctane (23 vol.%)
ETBEmax	EN 228 compliant blend, ETBE (22 vol.%)
FT(20)ETBE	EN 228 compliant blend, ETBE (22 vol.%), FT-Surrogate (20 vol.%)

First, iteratively performed auto-ignition simulations are used to determine the critical compression ratios, i.e., the compression ratio with the first occurrence of auto-ignition in the unburned zone. These results, characterizing the fuel's ignition behavior are related to their octane numbers and the polymerization of following equation:

$$RON = a \cdot x + b + \frac{c}{1 + \exp(-d \cdot (x - e))} + \frac{f}{1 + \exp(-g \cdot (x - h))} \quad (23)$$

results in a correlation which provides the connection of any fuel's simulated CCR to its octane number similar to the standardized method.

Due to the influence of the chemical kinetic mechanism on the ignition simulations, the derived correlations are tied to the mechanism used to generate them. As a consequence, the correlation function in Eq. (23) needs to be fitted individually for every new mechanism.

3. Results and discussion

The new implemented two-zone model for octane number prediction is calibrated against an experimental pressure curve. Coupled with chemical kinetic mechanisms, auto-ignition simulations can be performed to determine critical compression ratios, which are subsequently related to the octane number.

In a first model evaluation, the two-zone quasi-dimensional approach is compared with a correlation based on ignition delay times established by Badra et al. [17] for the analysis of TPRFs.

The ignition delay time simulations were performed in a zero-dimensional homogeneous reactor with constant temperature and pressure boundary conditions of 850 K and 50 atm, which according to Badra et al. [17], reflect well the standardized conditions for the research octane number.

With both methods, the fuel mixtures one through six listed in Table 1 were simulated using the gasoline surrogate mechanism of LLNL 2012 [40].

Fig. 4 demonstrates a clear correlations between the RON and the ignition delay times (left) and the CCR of the two-zone model (right). Regarding the PRFs and TPRFs, the results of the simple zero-dimensional model are in very good agreement with the plotted correlation introduced by Badra et al. [17]. However, the blends with ethanol are out of line and show a different trend, indicating that the heavily simplified boundary conditions of the zero-dimensional approach are not sufficient to simulate fuels with different compositions and molecules. In contrast, the quasi-dimensional approach shows clear advantages while maintaining reasonable numerical costs. The model reproduces the same trends for all fuels and demonstrates the advantages of the approach of calculating critical compression ratios leading to fuel-specific ignition conditions. The implementation of the second zone also allows the inclusion of the pressure increase from the burned gas and its influence on the secondary spontaneous ignition of the residual gas.

Below 90 RON the course is degressive and the correlation exhibits a sensitive behavior with respect to the compression ratio. An approximately linear correlation is observed when comparing the simulated CCR with the RON above 95 RON and in the range relevant for the application in gasoline engines. This allows the derivation of the correlation shown in the right figure, which can be well applied to the variety of fuels shown in Fig. 4. The parameter for the optimized correlation function Eq. (23) can be found in the Supplementary Material. A further comparison of the two-zone cylinder model against a zero-dimensional approach proposed by Westbrook et al. [18] using a predefined pressure profile is shown in the Supplementary Material. This approach shows a distinct correlation between the ignition delay times and the RON below 95 RON. For higher RON, higher divergence of the results is observed. Here, the zero-dimensional model is not capable to capture real engine boundary conditions sufficiently.

For a more detailed analysis and validation regarding various fuel classes, the two-zone model was applied to the fuel blends three through eight listed in Table 1 including toluene, ethanol and isobutanol. The simulations are performed using the gasoline surrogate mechanism LLNL 2020 [41]. The resulting critical compression ratios are plotted with the experimentally derived octane numbers in Fig. 5 on the left. On the right, the octane numbers using the derived correlation are compared to the values from literature. The results show a consistent pattern, demonstrating the model capability to predict octane numbers for a variety of different fuel blends. The deviations of all considered fuels, regardless of their composition, are in the range of ± 5 RON demonstrating the quality of the predictions. The accuracy of the predicted octane numbers for the simulated fuels with the ID No. 3 through 8 according to Table 1 can be rated by calculating the root mean square error (RMSE), which results in a value of 1.72 RON units.

Fig. 6 shows the results for CCR-RON and RON-RON correlations using the mechanism by POLIMI 2020 [42] for simulating the surrogates ID No. 3–6 and 9 from Table 1. The clear pattern that emerges again from the comparison of the simulated CCR with the experimental octane numbers demonstrates the flexibility of the two-zone model in utilizing and exchanging chemical kinetic mechanisms.

With the derived correlation applied on the fuels, the simulated octane numbers are mostly determined within ± 5 RON, proving the overall validity of the new two-zone cylinder model. The RMSE amounts to 3.1 RON units for the blends shown in Fig. 6 and 1.2 if the fuels with ETBE in their composition are excluded. It demonstrates its capability to handle different fuel blends with numerous components and is flexible in terms of applying different chemical kinetic mechanisms, allowing it to accommodate an even wider variety of fuels.

Within the data set series containing ETBE, there are two blends which slightly exceeds this ± 5 RON limit. Also other surrogate blends of PRF and ETBE show more distinct RON deviations compared to the fuels without ETBE, leading also to a higher RMSE. A reason for these systematic deviations could be model uncertainties of the POLIMI 2020 in the ETBE submodel. To our best knowledge there are no ignition delay time measurements in the low temperature regime for ETBE available in literature. Also other chemical kinetic investigations for the low temperature combustion of ETBE are limited. Dagaut et al. [46] investigated the oxidation of blends of n-heptane and ETBE in a jet stirred reactor (JSR). Fig. 7 left shows that the general reactivity of the blend as well as the peak concentrations of the intermediate species are in good agreement between experiment and model for higher temperatures above 800 K. Nevertheless, Fig. 7 right shows significant deviations between the experimental and modeling results for lower temperatures below 750 K. Here, the peak concentrations of the species CO_2 and C_2H_4 are overpredicted by the POLIMI 2020 model, indicating a too high reactivity of the low temperature combustion chemistry. This elevated reactivity also affects the simulated ignition behavior of the fuel blends containing ETBE executed within this work. This clearly shows, that further modeling investigations on the low temperature combustion of ETBE are required. These investigations need to be

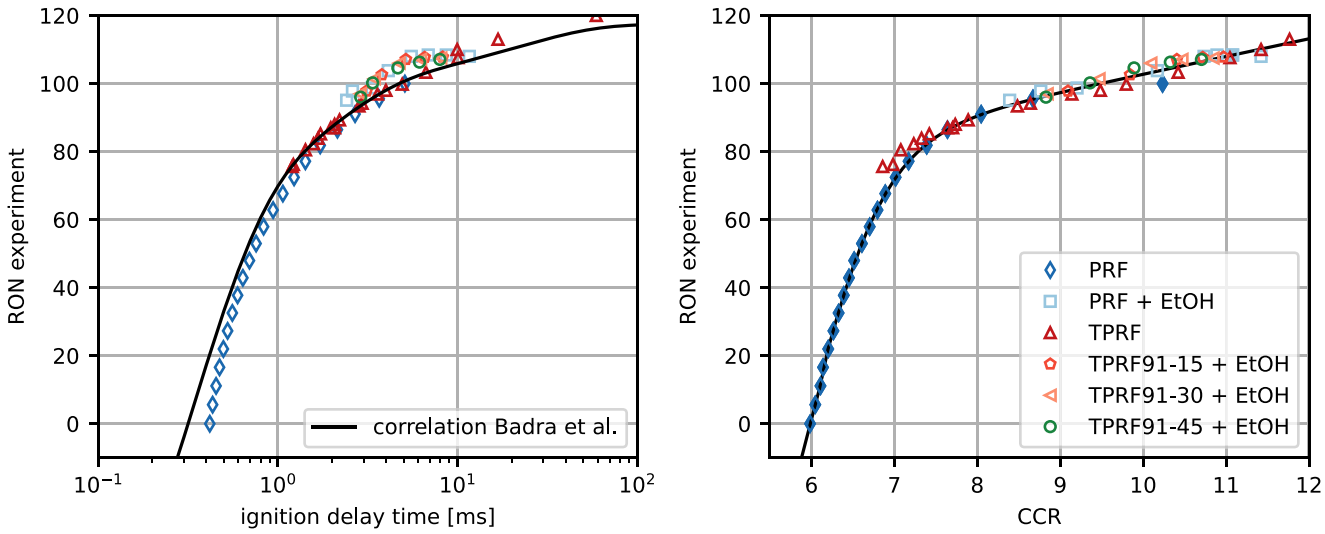

Fig. 4. Comparison of simulation results with experimentally determined octane numbers. Left: Ignition delay times obtained using a zero-dimensional approach with fixed boundary conditions. Right: Critical compression ratio obtained using the two-zone cylinder model. Filled markers indicate data points used to optimize the correlation function.

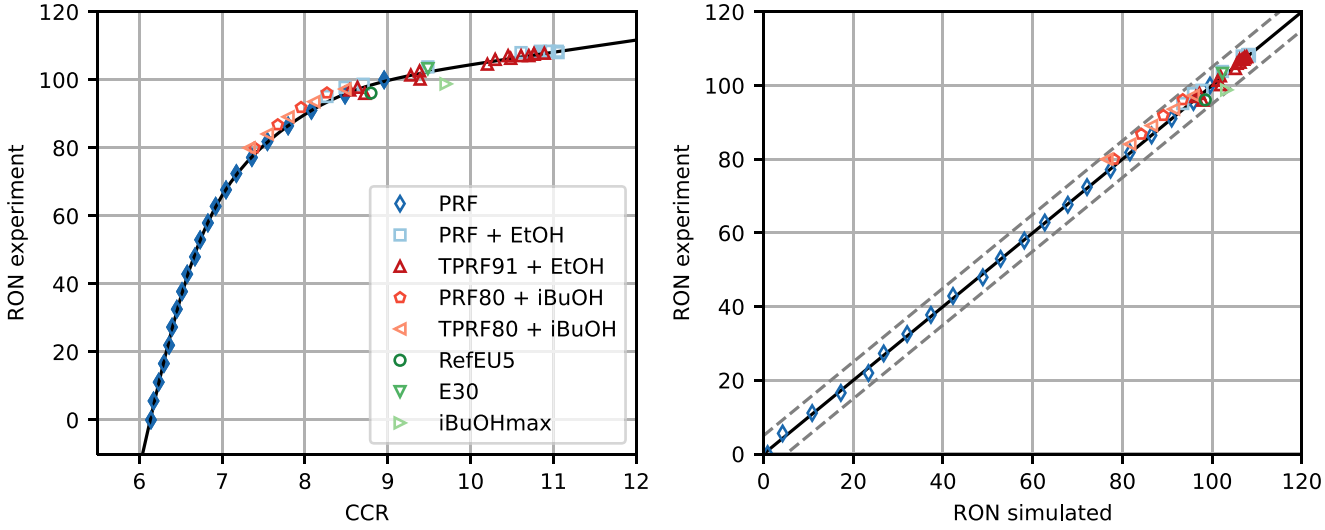

Fig. 5. Modeling results of the two-zone cylinder model using the LLNL 2020 mechanism. Left: Comparison between the experimentally derived octane number and the simulated critical compression ratio, the black line illustrates the established correlation. Filled markers indicate data points used to optimize the correlation function including the PRF datapoints and for better extrapolation beyond a octane number of 100 a PRF with 80 vol.% ethanol added. Right: Experimentally derived octane numbers compared to the octane number calculated using the correlation, the dashed lines visualize the range of ± 5 RON.

accompanied by further experimental chemical kinetic investigations, like ignition delay time measurements in rapid compression machines or shock tubes.

Cheng et al. [47] investigated the influence of kinetic models on simulations of engine spontaneous combustion and concluded that uncertainties in the reaction rates of kinetic models can lead to an uncertainty 14 times higher than the accuracy of the experimental setup. The uncertainty can be reduced by 60 percent by optimizing the kinetic models via fundamental experimental data like ignition delay times measurements. With this work, the significance of validated chemical kinetic models is demonstrated.

Other effects on the deviations between the predicted and measured RON are contributed by the simplifications of the two-zone model itself. As discussed before, the homogeneous modeling approach requires simplifications, firstly for the wall heat losses and secondly for the combustion rate. Turbulence combined with fuel dependent effects are modeled by a simplified scaling approach, due to limited flow information a homogeneous model. Also, the influence of cooling effects due to fuel specific enthalpies of vaporization are not implemented in the current model. Nevertheless, the overall good agreement between the numerical and experimental RON estimations justify these model simplifications and therefore, further model improvements were not the focus for this proof of concept.

A desirable goal is to predict the RON of real technical fuels consisting of a large number of different species. With the derived correlation and validation of the two-zone cylinder model with simple surrogate compositions, the octane numbers of different real fuels, listed in Table 2 were simulated.

The results are given in Table 3 and visualized in Fig. 5 when the LLNL 2020 is applied respectively in Fig. 6 when the kinetic model POLIMI 2020 is used. For the determination of the octane numbers of E30 and iBuOHmax as well as the RefEU5, the updated gasoline surrogate mechanism by LLNL 2020 [41] is applied. For all three fuels, the predicted RON lies within the prediction capability of ± 5 RON.

The octane numbers of the fuels ReMax, FT(20)ETBE and ETBEmax as well as the RefEU5 are determined by the simulation of the critical compression ratio using the chemical kinetic model POLIMI 2020. The result of RefEU5 fuel is well matched within the prediction interval of

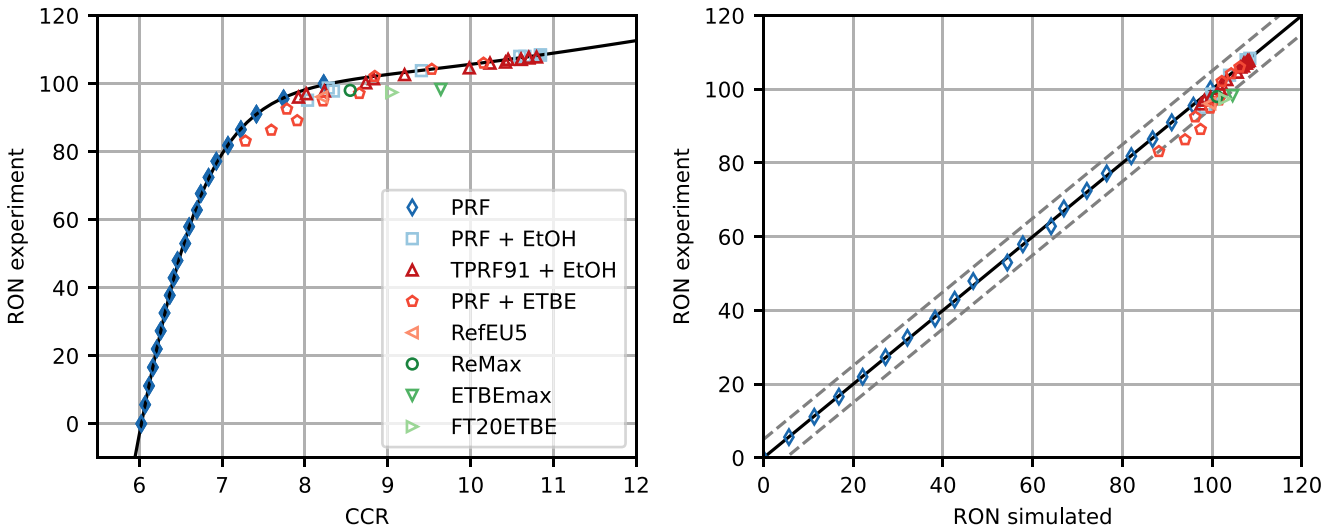

Fig. 6. Modeling results of the two-zone cylinder model using the POLIMI 2020 mechanism. Left: Comparison between the experimentally derived octane number and the simulated critical compression ratio. Filled markers indicate data points used to optimize the correlation function including the PRF datapoints and for better extrapolation beyond a octane number of 100 a PRF with 80 vol.% ethanol added. Right: Experimentally derived octane numbers compared to the octane numbers calculated using the derived correlation.

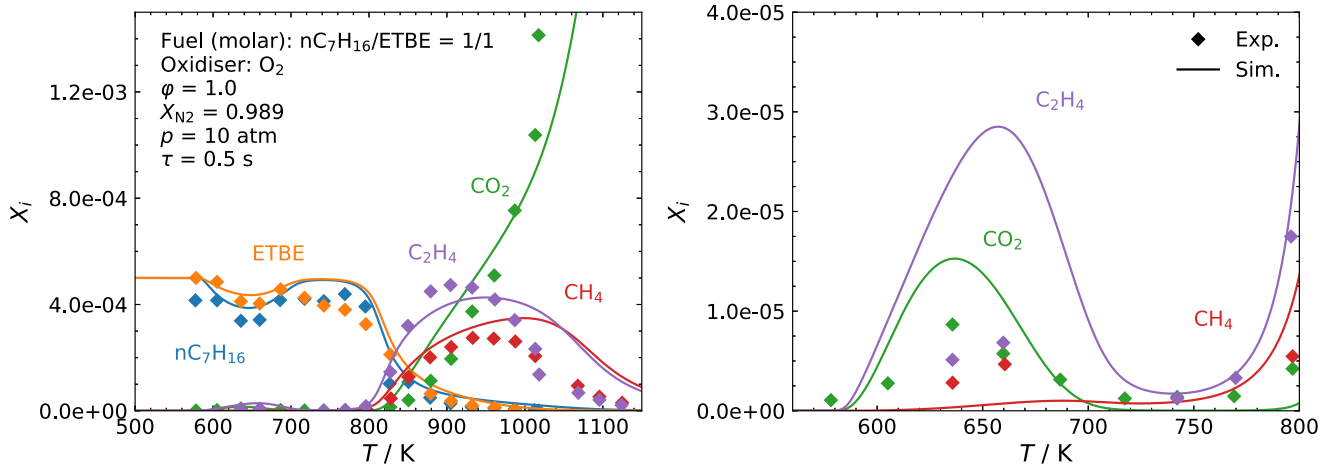

Fig. 7. Model performance of POLIMI 2020 for experimental species profiles from the oxidation of an n-heptane/ETBE blend in a JSR from Dagaut et al. [46], with the low temperature combustion regime visible below 750 K.

Table 3
Predicted octane number of real fuels.

Fuel, mechanism	RON experimental	RON simulated
RefEU5, LLNL 2020	96.1	98.5
E30, LLNL 2020	103.3	102.3
iBuOHmax, LLNL 2020	98.8	103.2
RefEU5, POLIMI 2020	96.1	99.5
ReMax, POLIMI 2020	98.0	101.1
ETBEmax, POLIMI 2020	98.3	104.6
FT(20)ETBE, POLIMI 2020	97.4	102.8

± 5 RON. However, the deviations in the results of ReMax, FT(20)ETBE and ETBEmax blends are larger with the octane numbers overestimated. The results of FT(20)ETBE and ETBEmax exceed the ± 5 RON window. This overestimation of the fuel blends is already evident in the results of the simple three-component PRF-ETBE surrogate, so further work is needed in the area of investigating the influence and validity of the ETBE submodel of the applied chemical kinetic mechanism.

4. Conclusions

A simplified two-zone cylinder model for the prediction of octane numbers was successfully developed, implemented in Cantera [33] and validated. The presented model does not depend on specific, experimentally derived fuel-specific input data such as pressure or predefined volume profiles. For great fuel flexibility, the model is designed for the chemical kinetic mechanisms to be interchangeable.

The two-zone model demonstrates an accurate predictive capability of research octane numbers for a broad range of fuel blends. All simulated fuels or their octane numbers are predicted within a range of ± 5 RON units. Only two fuel blends exceed these limits due to their ETBE content. The accuracy of the model using the LLNL [41] chemical kinetic mechanism is expressed by an RMSE value of 1.7 RON units. Using the kinetic model of POLIMI [42], the RMSE is 3.1, but drops to 1.2 when the fuels with ETBE content are excluded from this assessment, showing the potential for more accurate results by optimizing the chemical kinetic models. The simulation at typical piston motor boundary conditions clearly improves the predictive capability of this approach compared to simplified ignition delay time correlations from 0D approaches. This two-zone modeling approach demonstrates

a high interchangeability of implemented chemical kinetic models, allowing a flexible model application for versatile fuel blends. The numerical costs of the two-zone model are moderately increased compared to 0D approached and significantly reduced compared to fully three-dimensional CFD approaches. Thus, making the two-zone model efficiently applicable for extensive numerical tasks, like the screening of a large number of various fuels or fuel optimization processes.

Furthermore, multiple real fuel blends were tested, ranging from a pure fossil composition to blends with large proportions of renewable components including FT fractions as well as oxygenates. The results for these complex fuel blends agree well with the experimentally determined data and therefore provide additional proof of concept but also show the importance of validated chemical kinetic models.

With the predictive capabilities of the research octane number shown, the presented model will also be applied for the prediction of the motor octane number, as both quantities are of great importance for the application. Since the difference between research and engine octane number defines octane sensitivity, the combination of the prediction of both fuel properties is of particular interest.

With these application possibilities the presented two-zone cylinder model can support extensive technical fuel assessments and development of novel sustainable fuels.

Declaration of competing interest

The authors declare that they have no known competing financial interests or personal relationships that could have appeared to influence the work reported in this paper.

Acknowledgment

We thank the German Federal Ministry of Economic Affairs and Climate Action (BMWK) for financial support of this work within the project “Solare Kraftstoffe” [03EIV221].

Appendix A. Supplementary data

Supplementary material related to this article can be found online at https://doi.org/10.1016/j.jaecs.2022.100079.

References

[1] Leitner W, Klankermayer J, Pischinger S, Pitsch H, Kohse-Höinghaus K. Advanced biofuels and beyond: Chemistry solutions for propulsion and production. Angew Chem Int Ed Engl 2017;56(20):5412–52. http://dx.doi.org/10.1002/anie.201607257.

[2] Zinsmeister J, Gaiser N, Melder J, Bierkandt T, Hemberger P, Kasper T, et al. On the diversity of fossil and alternative gasoline combustion chemistry: A comparative flow reactor study. Combust Flame 2022;111961. http://dx.doi.org/10.1016/j.combustflame.2021.111961.

[3] Doliente SS, Narayan A, Tapia JFD, Samsatli NJ, Zhao Y, Samsatli S. Bio-aviation fuel: A comprehensive review and analysis of the supply chain components. Front Energy Res 2020;8. http://dx.doi.org/10.3389/fenrg.2020.00110.

[4] Dagaut P, Karsenty F, Dayma G, Diévart P, Hadj-Ali K, Mzé-Ahmed A, et al. Experimental and detailed kinetic model for the oxidation of a gas to liquid (GtL) jet fuel. Combust Flame 2014;161(3):835–47. http://dx.doi.org/10.1016/j.combustflame.2013.08.015.

[5] Oßwald P, Zinsmeister J, Kathrotia T, Alves-Fortunato M, Burger V, van der Westhuizen R, et al. Combustion kinetics of alternative jet fuels, Part-I: Experimental flow reactor study. Fuel 2021;302:120735. http://dx.doi.org/10.1016/j.fuel.2021.120735.

[6] Dreizler A, Pitsch H, Scherer V, Schulz C, Janicka J. The role of combustion science and technology in low and zero impact energy transformation processes. Appl Energy Combust Sci 2021;7:100040. http://dx.doi.org/10.1016/j.jaecs.2021.100040.

[7] Boot MD, Tian M, Hensen EJ, Sarathy SM. Impact of fuel molecular structure on auto-ignition behavior – Design rules for future high performance gasolines. Prog Energy Combust Sci 2017;60:1–25. http://dx.doi.org/10.1016/j.pecs.2016.12.001.

[8] Morgan N, Smallbone A, Bhave A, Kraft M, Cracknell R, Kalghatgi G. Mapping surrogate gasoline compositions into RON/MON space. Combust Flame 2010;157(6):1122–31. http://dx.doi.org/10.1016/j.combustflame.2010.02.003.

[9] Lugo HJ, Ragone G, Zambrano J. Correlations between octane numbers and catalytic cracking naphtha composition. Ind Eng Chem Res 1999;38(5):2171–6. http://dx.doi.org/10.1021/ie980273r.

[10] Ghosh P, Hickey KJ, Jaffe SB. Development of a detailed gasoline composition-based octane model. Ind Eng Chem Res 2005;45(1):337–45. http://dx.doi.org/10.1021/ie050811h.

[11] Nikolaou N, Papadopoulos C, Gaglias I, Pitarakis K. A new non-linear calculation method of isomerisation gasoline research octane number based on gas chromatographic data. Fuel 2004;83(4–5):517–23. http://dx.doi.org/10.1016/j.fuel.2003.09.011.

[12] Tipler S, Fürst M, Haute QV, Contino F, Coussement A. Prediction of the octane number: A Bayesian pseudo-component method. Energy Fuels 2020;34(10):12598–605. http://dx.doi.org/10.1021/acs.energyfuels.0c01700.

[13] Pal P, Kalvakala K, Wu Y, McNenly M, Lapointe S, Whitesides R, et al. Numerical investigation of a central fuel property hypothesis under boosted spark-ignition conditions. In: ASME 2019 internal combustion engine division fall technical conference. American Society of Mechanical Engineers; 2019, http://dx.doi.org/10.1115/ICEF2019-7284.

[14] Li R, Herreros JM, Tsolakis A, Yang W. Machine learning regression based group contribution method for cetane and octane numbers prediction of pure fuel compounds and mixtures. Fuel 2020;280:118589. http://dx.doi.org/10.1016/j.fuel.2020.118589.

[15] vom Lehn F, Brosius B, Broda R, Cai L, Pitsch H. Using machine learning with target-specific feature sets for structure-property relationship modeling of octane numbers and octane sensitivity. Fuel 2020;281:118772. http://dx.doi.org/10.1016/j.fuel.2020.118772.

[16] vom Lehn F, Cai L, Tripathi R, Broda R, Pitsch H. A property database of fuel compounds with emphasis on spark-ignition engine applications. Appl Energy Combust Sci 2021;5:100018. http://dx.doi.org/10.1016/j.jaecs.2020.100018.

[17] Badra JA, Bokhumseen N, Mulla N, Sarathy SM, Farooq A, Kalghatgi G, et al. A methodology to relate octane numbers of binary and ternary n-heptane, iso-octane and toluene mixtures with simulated ignition delay times. Fuel 2015;160:458–69. http://dx.doi.org/10.1016/j.fuel.2015.08.007.

[18] Westbrook C, Sjöberg M, Cernansky N. A new chemical kinetic method of determining RON and MON values for single component and multicomponent mixtures of engine fuels. Combust Flame 2018;195:50–62. http://dx.doi.org/10.1016/j.combustflame.2018.03.038.

[19] Fioroni GM, Rahimi MJ, Westbrook CK, Wagnon SW, Pitz WJ, Kim S, et al. Chemical kinetic basis of synergistic blending for research octane number. Fuel 2022;307:121865. http://dx.doi.org/10.1016/j.fuel.2021.121865.

[20] Curran HJ, Gaffuri P, Pitz WJ, Westbrook CK, Leppard WR. Autoignition chemistry in a motored engine: An experimental and kinetic modeling study. Symp (Int) Combust 1996;26(2):2669–77. http://dx.doi.org/10.1016/S0082-0784(96)80102-0.

[21] Callahan C, Held T, Dryer F, Minetti R, Ribaucour M, Sochet L, et al. Experimental data and kinetic modeling of primary reference fuel mixtures. Symp (Int) Combust 1996;26(1):739–46. http://dx.doi.org/10.1016/S0082-0784(96)80282-7.

[22] Zhang P, Yee NW, Filip SV, Hetrick CE, Yang B, Green WH. Modeling study of the anti-knock tendency of substituted phenols as additives: an application of the reaction mechanism generator (RMG). Phys Chem Chem Phys 2018;20(16):10637–49. http://dx.doi.org/10.1039/c7cp07058f.

[23] Pal P, Kolodziej CP, Choi S, Som S, Broatch A, Gomez-Soriano J, et al. Development of a virtual CFR engine model for knocking combustion analysis. SAE Int J Eng 2018;11(6):1069–82. http://dx.doi.org/10.4271/2018-01-0187.

[24] Pal P, Wu Y, Lu T, Som S, See YC, Moine AL. Multidimensional numerical simulations of knocking combustion in a cooperative fuel research engine. J Energy Resour Technol 2018;140(10). http://dx.doi.org/10.1115/1.4040063.

[25] Hajireza S, Mauss F, Sundén B. Hot-spot autoignition in spark ignition engines. Proc Combust Inst 2000;28(1):1169–75. http://dx.doi.org/10.1016/s0082-0784(00)80327-6.

[26] Perini F, Paltrinieri F, Mattarelli E. A quasi-dimensional combustion model for performance and emissions of SI engines running on hydrogen–methane blends. Int J Hydrogen Energy 2010;35(10):4687–701. http://dx.doi.org/10.1016/j.ijhydene.2010.02.083.

[27] Foong TM. On the autoignition of ethanol/gasoline blends in spark-ignition engines (Ph.D. thesis), The Department of Mechanical Engineering The University of Melbourne; 2013.

[28] Gamma Technologies, GT-power user’s manual, version 7.3. 2012.

[29] Woschni G. A univerally applicable equation for the instantaneous heat transfer coefficient in the interal combustion engine. 1968, SAE Transactions 76: 3065-83.

[30] Mehl M, Faravelli T, Giavazzi F, Ranzi E, Scorletti P, Tardani A, et al. Detailed chemistry promotes understanding of octane numbers and gasoline sensitivity. Energy Fuels 2006;20(6):2391–8. http://dx.doi.org/10.1021/ef060339s.

[31] Jürgens S, Oßwald P, Selinsek M, Piermartini P, Schwab J, Pfeifer P, et al. Assessment of combustion properties of non-hydroprocessed Fischer-Tropsch fuels for aviation. Fuel Process Technol 2019;193:232–43. http://dx.doi.org/10.1016/j.fuproc.2019.05.015.

[32] Dieterich V, Buttler A, Hanel A, Spliethoff H, Fendt S. Power-to-liquid via synthesis of methanol, DME or Fischer–Tropsch-fuels: a review. Energy Environ Sci 2020;13(10):3207–52. http://dx.doi.org/10.1039/D0EE01187H.

[33] Goodwin DG, Moffat HK, Schoegl I, Speth RL, Weber BW. Cantera: An object-oriented software toolkit for chemical kinetics, thermodynamics, and transport processes. 2022, http://dx.doi.org/10.5281/zenodo.6387882, Zenodo.
[34] Mittal G, jen Sung C. A rapid compression machine for chemicalkinetics studies at elevated pressures and temperatures. Combust Sci Technol 2007;179(3):497–530. http://dx.doi.org/10.1080/00102200600671898.
[35] Kee RJ, Coltrin ME, Glarborg P, Zhu H. Chemically reacting flow: theory, modeling, and simulation. John Wiley & Sons; 2017.
[36] Verhelst S, Sheppard C. Multi-zone thermodynamic modelling of spark-ignition engine combustion – An overview. Energy Convers Manage 2009;50(5):1326–35. http://dx.doi.org/10.1016/j.enconman.2009.01.002.
[37] Yasar H, Soyhan H, Walmsley H, Head B, Sorusbay C. Double-wiebe function: An approach for single-zone HCCI engine modeling. Appl Therm Eng 2008;28(11–12):1284–90. http://dx.doi.org/10.1016/j.applthermaleng.2007.10.014.
[38] Han Z, Reitz RD. A temperature wall function formulation for variable-density turbulent flows with application to engine convective heat transfer modeling. Int J Heat Mass Transfer 1997;40(3):613–25. http://dx.doi.org/10.1016/0017-9310(96)00117-2.
[39] Elliott L, Ingham D, Kyne A, Mera N, Pourkashanian M, Wilson C. Genetic algorithms for optimisation of chemical kinetics reaction mechanisms. Prog Energy Combust Sci 2004;30(3):297–328. http://dx.doi.org/10.1016/j.pecs.2004.02.002.
[40] Mehl M, Pitz WJ, Westbrook CK, Curran HJ. Kinetic modeling of gasoline surrogate components and mixtures under engine conditions. Proc Combust Inst 2011;33(1):193–200. http://dx.doi.org/10.1016/j.proci.2010.05.027.
[41] Cheng S, Saggese C, Kang D, Goldsborough SS, Wagnon SW, Kukkadapu G, et al. Autoignition and preliminary heat release of gasoline surrogates and their blends with ethanol at engine-relevant conditions: Experiments and comprehensive kinetic modeling. Combust Flame 2021;228:57–77. http://dx.doi.org/10.1016/j.combustflame.2021.01.033.
[42] Pelucchi M, Cavallotti C, Faravelli T, Klippenstein SJ. H-abstraction reactions by OH, HO_2, O, O_2 and benzyl radical addition to O_2 and their implications for kinetic modelling of toluene oxidation. Phys Chem Chem Phys 2018;20(16):10607–27. http://dx.doi.org/10.1039/C7CP07779C.
[43] Fan Y, Duan Y, Han D, Qiao X, Huang Z. Influences of isomeric butanol addition on anti-knock tendency of primary reference fuel and toluene primary reference fuel gasoline surrogates. Int J Engine Res 2019;22(1):39–49. http://dx.doi.org/10.1177/1468087419850704.
[44] Ogura T, Sakai Y, Miyoshi A, Koshi M, Dagaut P. Modeling of the oxidation of primary reference fuel in the presence of oxygenated octane improvers: Ethyl Tert-Butyl ether and ethanol. Energy Fuels 2007;21(6):3233–9. http://dx.doi.org/10.1021/ef700321e.
[45] Kathrotia T, Oßwald P, Zinsmeister J, Methling T, Köhler M. Combustion kinetics of alternative jet fuels, Part-III: Fuel modeling and surrogate strategy. Fuel 2021;302:120737. http://dx.doi.org/10.1016/j.fuel.2021.120737.
[46] Dagaut P, Koch R, Cathonnet M. The oxidation of N-heptane in the presence of oxygenated octane improvers: MTBE and ETBE. Combust Sci Technol 1997;122(1–6):345–61. http://dx.doi.org/10.1080/00102209708935615.
[47] Cheng S, Yang Y, Brear MJ, Frenklach M. Quantifying uncertainty in kinetic simulation of engine autoignition. Combust Flame 2020;216:174–84. http://dx.doi.org/10.1016/j.combustflame.2020.02.025.